JOURNAL OF THE KOREAN ASTRONOMICAL SOCIETY
30: 71 ~ 81, 1997

IR CHARACTERISTICS OF MOLECULAR CLOUDS IN THE REGION OF SUPERSHELL GS234–02

JUNG, JAE HOON[1], LEE, JUNG KYU[2] AND YOON, TAE SEOG[2]
[1]Korea Astronomy Observatory, Taejeon 305-348, Korea; jhjung@hanul.issa.re.kr
[2]Department of Astronomy and Atmospheric Sciences, Kyungpook National University, 702-701, Korea
(Received Mar. 28, 1997; Accepted Apr. 18, 1997)

ABSTRACT

We have studied the IR properties of molecular clouds in the region of the supershell GS234−02 using IRAS and COBE data. The mean values of dust color temperature and optical depth at 240μm are derived to be 15.4 ± 1.5 K and $9.0 \pm 5.7 \times 10^{-4}$, respectively, which agree well with those determined by Sodroski *et al.*(1994) for the outer Galaxy. Mean IRAS colors, $R_{12/100}$= 0.074, $R_{25/100}$= 0.052, $R_{60/100}$= 0.219, indicate that the abundance of PAHs is enhanced but other particles are nearly the same as those of the solar neighborhood. We found the anticorrelation between $R_{100/140}$ and $R_{140/240}$. It cannot be explained by the thermal emission of traditional big grains. The anticorrelation implies that, at high ISRF, $T_{100/140}$ underestimates the equilibrium temperature, while $T_{140/240}$ overestimates it and, at low ISRF, vice versa. Therefore we propose to use the intensity ratio, $R_{100/240}$ as a dust thermometer.

Key Words : dust — infrared radiation— molecular clouds:GS234−02

I. INTRODUCTION

Infrared (IR) emission arises from the dust heated by the general interstellar radiation field (ISRF) of the Galaxy. Desert, Boulanger, & Puget (1990; hereinafter DBP) suggested that there should be at least three types of dust grain, i.e., Polycyclic Aromatic Hydrocarbon molecules (PAHs), Very Small Grains (VSGs), and Big Grains (BGs) in order to explain the observed extinction curve and the IR spectrum. Since the emission peaks of PAHs and VSGs are located near 12 and 60 μm, respectively (DBP), the IR colors such as the ratios of 12 μm to 100 μm and 60 μm to 100 μm can trace the abundance of each particle (Puget 1989).

Infrared Astronomical Satellite (IRAS) observations of molecular clouds (Weiland *et al.* 1986; Boulanger & Perault 1988; Heiles, Reach, & Koo 1988; Beichman *et al.* 1988; Laureijs *et al.* 1989; Boulanger *et al.* 1990) showed that there exist large variations of IR colors and limb-brightening. Theoretical calculations (DBP; Bernard *et al.* 1992) also showed that the mid-IR colors could be enhanced in weak ISRF, but the observed large variations up to a factor of 10 could not be explained by the change of ISRF only. Boulanger *et al.*(1990) suggested that the color variations between clouds or within a cloud are due to the abundance variations of small particles rather than ISRF.

On the other hand, the dust temperature derived from IRAS 60 and 100 μm appeared to be high compared with that estimated from dust model calculations or from molecular observations (Laureijs, Clark, & Prusti 1991, and references therein). This result was interpreted by the stochastic heating of VSGs at 60 μm (DBP). That is, small particles are heated to high temperature by absorbing UV photons and emit more radiation than expected from thermal equilibrium. But Sodroski *et al.*(1994) showed that dust temperature determined from far-IR (FIR) agreed well with that inferred from theoretical calculations or radio observations. This result implies that FIR colors can be used as a temperature indicator of dust which is in equilibrium with ISRF. However the heating mechanism, the equilibrium temperature, and the abundance of dust grains associated with molecular clouds are not clear, even though much portion, 15-30% (Sodroski *et al.*1989; Sodroski *et al.*1994), of the Galactic IR emission comes from

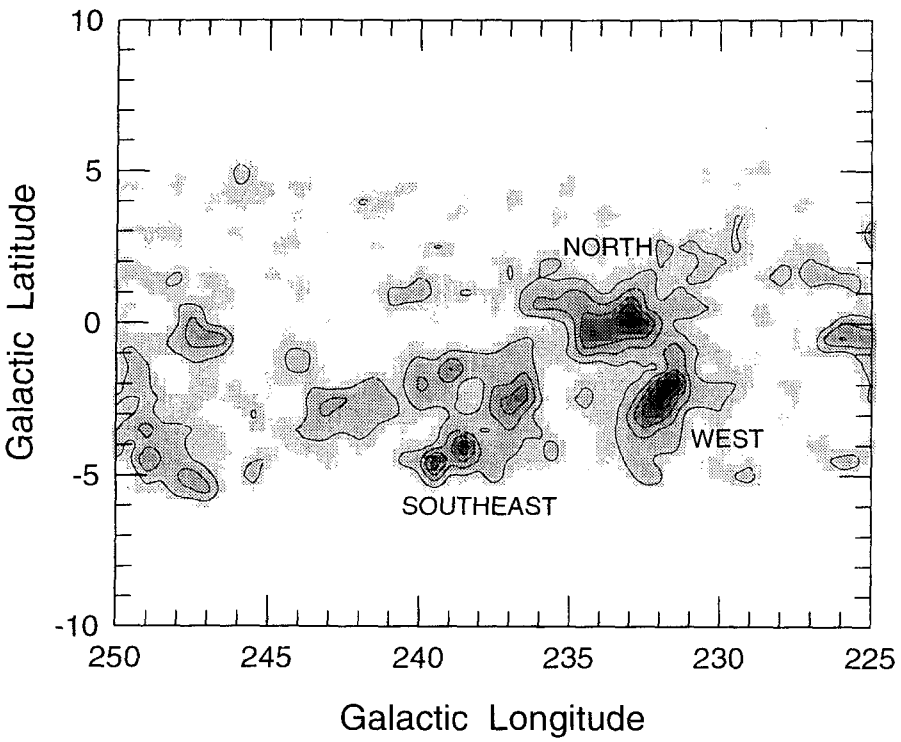

Fig. 1. ^{12}CO integrated intensity map between v_{LSR}=+15 and 56 km s^{-1} from May et al. (1988). The lowest contour is 1.5 K km s^{-1}, and the contour interval is 1.5 K km s^{-1}.

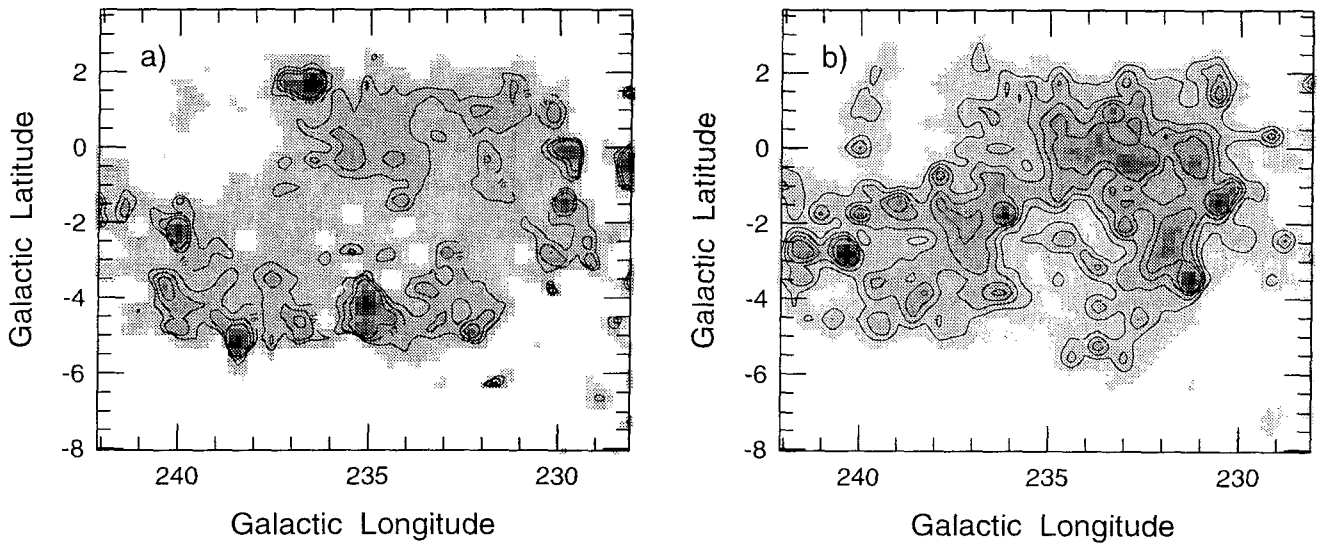

Fig. 2. Distributions of dust temperature and optical depth at 240 μm. a) Contour level begins from 16 K with intervals of 1 K. Gray image is on a linear scale over the temperature range from 12 to 23 K. b) Contour level begins from 4×10^{-4} with intervals of 2×10^{-4}. Gray image is on a linear scale over the optical depth range from 1×10^{-5} to 2×10^{-3}.

molecular clouds.

GS234−02 is a part of prominent IR loop structure of Sch235-03 (Schwartz 1987). Recently, Jung, Koo, & Kang (1996) made an extensive study of this loop structure with large-scale observational data of IR, *HI*, and CO. They suggested that the loop may be formed by the overlap of unrelated two components (see Figure 1); the southeastern

part is a diffuse nebula which is seen bright in Hα (Sivans 1974), whereas the northwestern one is an expanding supershell where the star formation is going on. They also showed that each component is composed of molecular clouds at different distances of 2.5 and 4 kpc. Moreover the northern part of the supershell is an active star forming region, while the western one is relatively a quiet one. Therefore the IR loop in the region of GS234−02 is a good candidate to examine the IR properties of molecular clouds which are exposed to different ISRF.

The aim of this study is to deduce the dust abundance from IR colors and to examine the dust equilibrium temperature of molecular clouds in the region of GS234−02. IRAS data and the Diffuse IR Background Experiment (DIRBE) of Cosmic Background Explorer (COBE) data are analyzed in section 2. IR colors are derived and compared with those calculated by dust model in section 3. We discuss the equilibrium temperature in section 4, and summarize our results in section 5.

II. DATA ANALYSIS

(a) Data

The data used here are IRAS 12, 25, 60 and 100 μm, and COBE 60, 100, 140, and 240 μm. IRAS and COBE data were obtained from the coadded images of IRAS Sky Survey Atlas (ISSA) and DIRBE Initial Data product. To reduce the effects of IRAS point sources and to compare the physical properties derived from the IRAS data with those from the COBE data, seven pixels of IRAS data were averaged. The size of an averaged pixel is 10.′5, which is a half of the pixel size of COBE. We checked the effect of averaging by comparing the IR colors derived from ISSA (1.′5) with those from averaged data (10.′5). The averaging process reduced the large scatter of IR colors near IRAS point sources and HII regions, but the mean values of IR colors appeared to be same. Therefore the general characteristics of our results are not affected by the averaging process.

In order to measure the net infrared emission of source, flat background corrections were performed with the background emission determined from source free regions (see Table 2 of Jung *et al.*. [1996] for detail). The calibration of IRAS experiments for extended emission is significantly different from that of DIRBE. Thus IRAS brightness were multiplied to agree with DIRBE measurements by the mean gain factors (Wheelock *et al.*1994), i.e., 1.06, 1.01, 0.87, and 0.72 for 12, 25, 60, and 100 μm. But we did not make any color corrections.

(b) Decomposition of Source and Derivation of Physical Parameters

As we introduced in section 1, GS234−02 region is composed of four molecular clouds (see Table 3 of Jung *et al.*1996). We reproduce the molecular gas distribution in Figure 1. Based on this map, we divide the region into three parts; northern, western, and southeastern part. Northern part is composed of the HII regions, S302, S305, S306, S307, and S309, where S302 (north1 in Table 1) is separated from other HII regions (north2) being the short distance. Western part is a dark cloud which contains no HII region except a few bright IRAS point sources. Southeastern part shows diffuse nebulosity in a POSS red print and contains BBW17, BBW22, BBW23, BBW29, BBW31, BBW44, BBW46, and BBW54.

After background and gain corrections, color temperature and optical depth are calculated pixel by pixel with the emissivity law of λ^{-2}. In deriving the optical depth, we use $\tau_\lambda = I_\lambda/B_\lambda(T)$ relation assuming that the optical depth is small enough. The derived mean values are listed in Table 1. In Table 1, columns (1) and (2) denote the selected region and the boundary of each region in galactic coordinate. Columns (3), (4), and (5) give the mean color temperatures derived from the intensity ratio between 60 and 100 μm ($T_{60/100}$), 100 and 140 μm ($T_{100/140}$), and 140 and 240 μm ($T_{140/240}$). Columns (6) and (7) represent the optical depths derived at 100 μm (τ_{100}) and 240 μm (τ_{240}) using $T_{60/100}$ and $T_{140/240}$, respectively. The mean values of color temperature and optical depth at 240 μm in west region, $T_{140/240}$= 15.4 ± 1.5 K and $\tau_{240} = 9.0 \pm 5.7 \times 10^{-4}$, are not much different from those (17±1 K, 9.7±3.0 × 10^{-4}) of general interstellar medium in the outer Galaxy (Sodroski *et al.*1994). In spite of the difference in ISRF, mean dust temperatures show no difference among regions. It may be due to the large pixel size of the DIRBE data (21′) compared with the extent of HII regions ($\lesssim$ 10′). In other words a large fraction of the IR emission comes from surrounding molecular clouds so that the IR colors represent the characteristics of the molecular clouds rather than that of the HII regions. The optical depth of southeast region (6.8±4.3 × 10^{-4}) is

Table 1. Color temperatures and optical depths of each region

	position (deg)		$T_{3/4}$ (K)		$T_{4/5}$ (K)	$T_{5/6}$ (K)	τ_{100}	τ_{240}
Region	$(l_1 : l_2)$	$(b_1 : b_2)$	IRAS	COBE			IRAS	COBE
North1	(232.1:233.1)	(0.5:1.2)	25.2±2.3	28.3±2.2	17.4±2.0	16.4±1.1	$2.0\pm0.5 \times 10^{-4}$	$8.3\pm3.0 \times 10^{-4}$
North2	(233.1:235.2)	(−1.2:1.2)	24.4±1.4	25.8±1.5	15.9±1.3	16.1±1.3	$2.3\pm0.8 \times 10^{-4}$	$9.7\pm3.7 \times 10^{-4}$
Southeast	(235.9:239.8)	(−5.1:−0.9)	24.2±1.3	24.2±2.0	15.7±1.5	15.8±1.6	$1.4\pm0.4 \times 10^{-4}$	$6.9\pm4.0 \times 10^{-4}$
West	(230.3:233.1)	(−4.0:0.5)	23.7±0.5	24.9±0.8	15.8±2.2	15.4±1.5	$1.7\pm0.4 \times 10^{-4}$	$9.0\pm5.7 \times 10^{-4}$

Table 2. Averaged colors of molecular clouds

region	$R_{12/100}$	$R_{25/100}$	$R_{60/100}$
West	0.075±0.007	0.060±0.008	0.222±0.022
Southeast			
total mean	0.071±0.014	0.062±0.022	0.240±0.047
high ISRF	0.058±0.010	0.076±0.013	0.282±0.024
low ISRF	0.077±0.008	0.045±0.011	0.206±0.033
North^{+}	0.070±0.008	0.051±0.013	0.230±0.016
Solar neighborhood^{++}	0.042±0.012	0.054±0.016	0.21±0.01

Notes to TABLE 2.

$^{+}$: averaged for $R_{60/100} \leq 0.25$

$^{++}$: data from Boulanger et al. (1990)

slightly less than those of other regions. Figure 1 also shows that the southeastern cloud is less dense than others. On the other hand, Table 1 shows that $T_{60/100}$ is much higher ($\Delta T \simeq 8$ K) than other color temperatures ($T_{100/140}$ and $T_{140/240}$), but there is no systematic difference between $T_{60/100}$ derived from IRAS and COBE. High $T_{60/100}$ suggests that VSGs contribute significantly to 60 μm emission. Thus $T_{60/100}$ is far from the equilibrium temperature of dust as pointed out by Terebey & Fich (1986).

Figure 2 shows the distributions of dust temperature and optical depth at 240 μm. In Figure 2a, high temperature regions are related with HII regions or bright IRAS point sources rather than rim-brightening, although the poor space resolution (0.°7) of COBE make it difficult to distinguish them. The optical depth map (Figure 2b) shows a clear loop structure, which corresponds very well with the molecular gas distribution. It implies that most FIR emission arises from the dust grains in molecular gas.

III. IR COLORS AND IMPLICATIONS

It has been suggested that each of the four IRAS bands samples the emission from a different type of particles (Puget *et al.*. 1985; Drain & Anderson 1985; Chlewicki & Laureijs 1988; DBP). Therefore IR colors can be used to deduce the abundance of each particles. However the mid-IR colors could be biased to large values by the limb-brightening usually appeared in molecular clouds (Beichman *et al.* 1988; Laureijs *et al.* 1989; Boulanger *et al.* 1990). The limb-brightening effect was examined by plotting the dependence of intensity ratios of 12 and 25 μm to 100 μm

on 100 μm intensity in Figure 3. The constant ratios with respect to 100 μm suggest no limb-brightening effect in the sampled clouds. Note that two groups appeared in Figure 3d and 3f: one has higher $R_{25/100}$ and the other has lower value. The former group may result from the heating by HII regions (see next).

IR colors were obtained pixel by pixel from IRAS and COBE data for each region. The observed IR colors from IRAS data are plotted in Figure 4, and are compared with the theoretical colors of cirrus cloud in different ISRF (DBP) which are plotted as a solid line in Figure 4. The reason why we choose the cirrus model is that the clouds have filamentary structure of several clumps of 10′ in high resolution observations of CO (Jung 1996), which is comparable to the averaged pixel size. It suggests that most IR emission comes from diffuse part of clouds whose mean visual extinction is derived to be less than 2 mag from I_{100}/A_V relation (Boulanger *et al.*1990). The mean values of IRAS colors for each region are listed in Table 2 where $R_{i/j}$ denotes intensity ratio of i band to j band of IRAS. Since the southeast region (Figure 4d) shows distinctive two groups, the mean values of IR colors are estimated separately for each group. The group with the large values of $R_{25/100}$ and $R_{60/100}$ may represent HII regions, whereas the other represents the clouds without internal heating sources. In north region, we take an average of IR colors only for pixels with $R_{60/100} \leq 0.25$, since these pixels show less destruction of PAHs and may represent the characteristics of dark molecular cloud.

Figure 4 shows that the observed $R_{25/100}$ agree well with the theoretical ones of low IRSF. But $R_{12/100}$ is higher than the theoretical one. Table 2 also shows that the mean value of $R_{12/100}= 0.074$ from all regions is about two times larger than that of the solar neighborhood, while $R_{25/100}$ and $R_{60/100}$ are nearly the same as those of the solar neighborhood within the observational error. There are several examples of large value of $R_{12/100}$ (Boulanger & Perault 1988; Laureijs *et al.*1989; Boulanger *et al.*1990), although $R_{12/100}$ varies widely from cloud to cloud, or varies by a factor of 10 even within a cloud. The large value of $R_{12/100}$ might be due to the high abundance of PAHs, or due to low ISRF (Boulanger *et al.*1990; DBP). If the clouds have the same dust composition and size spectrum as those of the solar neighborhood, same increments of $R_{12/100}$ and $R_{25/100}$ are expected in low ISRF as the theoretical calculation (DBP) shows. The observed $R_{12/100}$, however, is larger than that of model, while $R_{25/100}$ agrees well with the model. Therefore the large value of $R_{12/100}$ is an indication of the high abundance of PAHs rather than the low ISRF. Boulanger *et al.*(1990) also suggested that the color variations trace variations in the abundance of transiently heated particles.

An interesting feature of Figure 4 is the separation of $R_{25/100}$ in southeast region (Figure 4d, or Figure 3d). This separation may be due to the high excitation of VSGs. That is, the southeast region contains several HII regions, and VSGs near and/or in HII regions are heated to high temperature and radiate more energy than that expected from theoretical calculations at 25 μm. But this effect is not apparent in the north region (Figure 4f). This difference seems to be the result of the difference in dust opacity between two regions. The north region is much opaque than the southeast as shown in Table 1, and the cloud in the north region shields UV photon more effectively. If then, most 25 μm emission comes from the dust grains inside the cooler cloud and will not exhibit the separation. However, $R_{12/100}$ (Figure 4c) shows gradual decrease with $R_{60/100}$ rather than separation. This indicates the destruction of PAHs in high ISRF. There are several good examples of destruction of PAHs in HII regions (DBP; Werner and Gautier 1994). For comparison, color-color diagrams of DBP's model for HII region are plotted as a dot-long dashed line in Figures 4c - 4f. The disagreement of $R_{12/100}$ between the dust model and the observations at high $R_{60/100}$ appeared in Figure 4e shows the evidence of destruction of PAHs, but good agreement in $R_{25/100}$ suggests the stability of VSGs in high ISRF.

To see the effect of VSGs at 60 and 100 μm, we plot the colors derived from COBE data in Figure 5. In Figure 5, the colors determined from the cirrus model of DBP are also plotted with a solid (BGs only) and a dashed (VSGs + BGs) line. Here the intensities of 140 and 240 μm are calculated by interpolation, since DBP did not give the intensities at those frequencies. Figure 5 shows that BGs only cannot account the observed results at 60 μm, but relatively well at 100 μm. This indicates that much portion of 60 μm emission comes from VSGs and the contribution of VSGs becomes negligible at 100 μm. On the other hand, Figure 5e shows the large enhancement of 60 μm emission in HII regions. This may be an indication of strong UV field in the north region compared with southeast region. Puget (1989) suggested that $R_{60/100}$ is a tracer of the energy density of the UV field in HII region, where the 60 μm emission is mostly due to BGs.

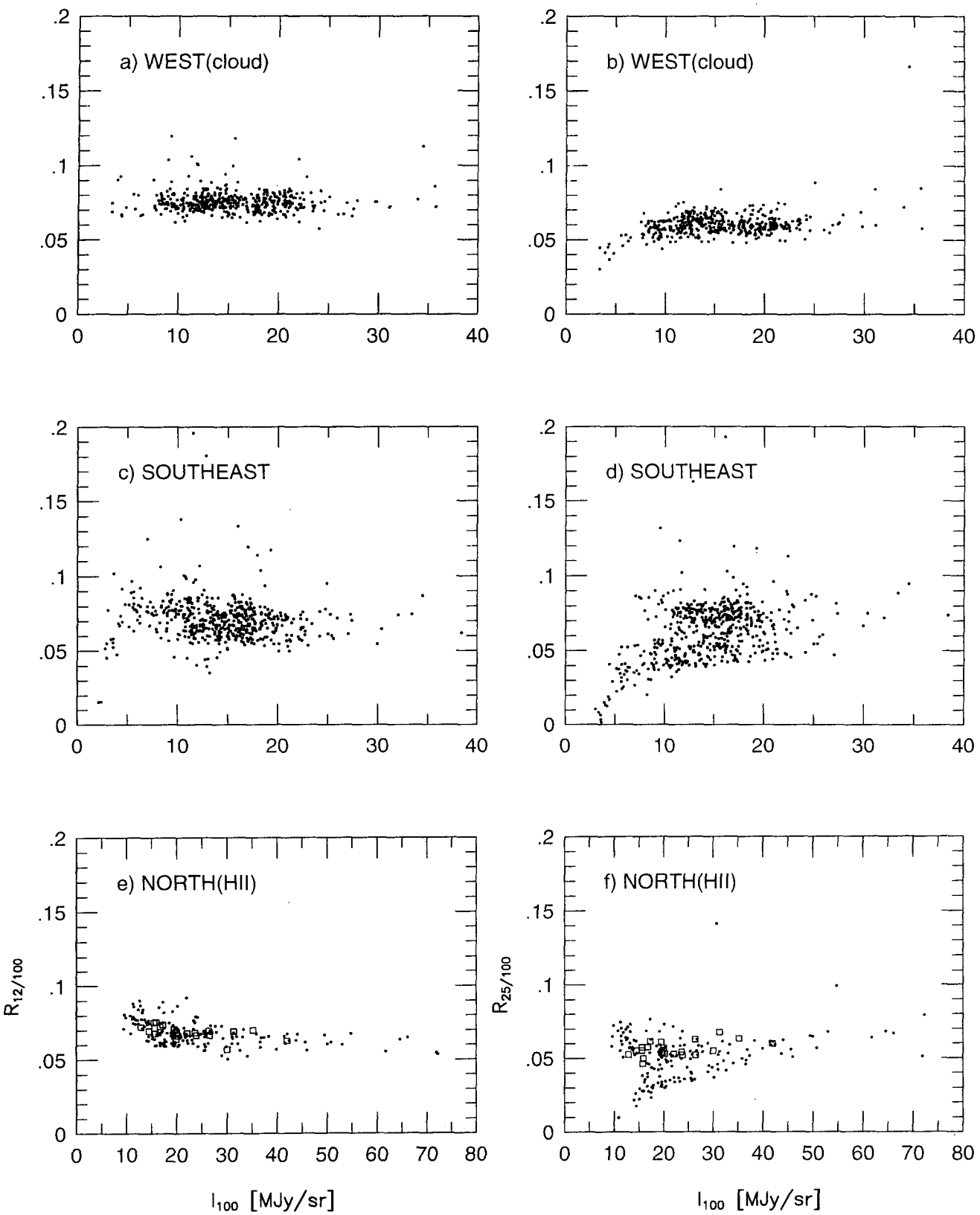

Fig. 3. Color variations as a function of 100 μm intensity. High 100 μm intensity corresponds to dense region. Notice the separation appeared in d) (see text).

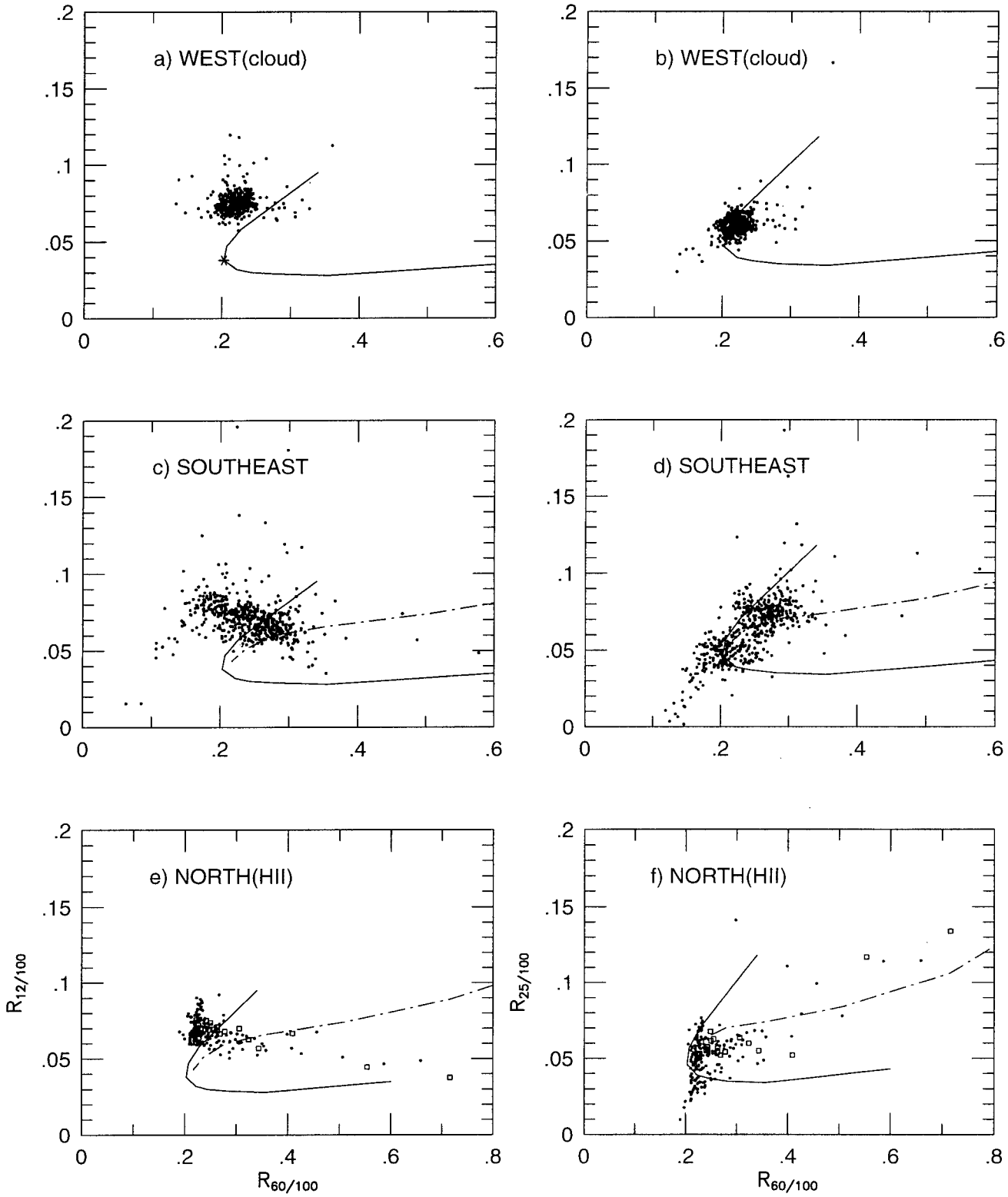

Fig. 4. Plots of near IR colors for each region. A solid line represents the color variations of cirrus clouds in different ISRF, and a dot-long dashed line HII regions (Desert, Boulanger, & Puget 1990). In a), an asterisk is the position of solar neighborhood. The open squares in e) and f) denote the data from the north1 region.

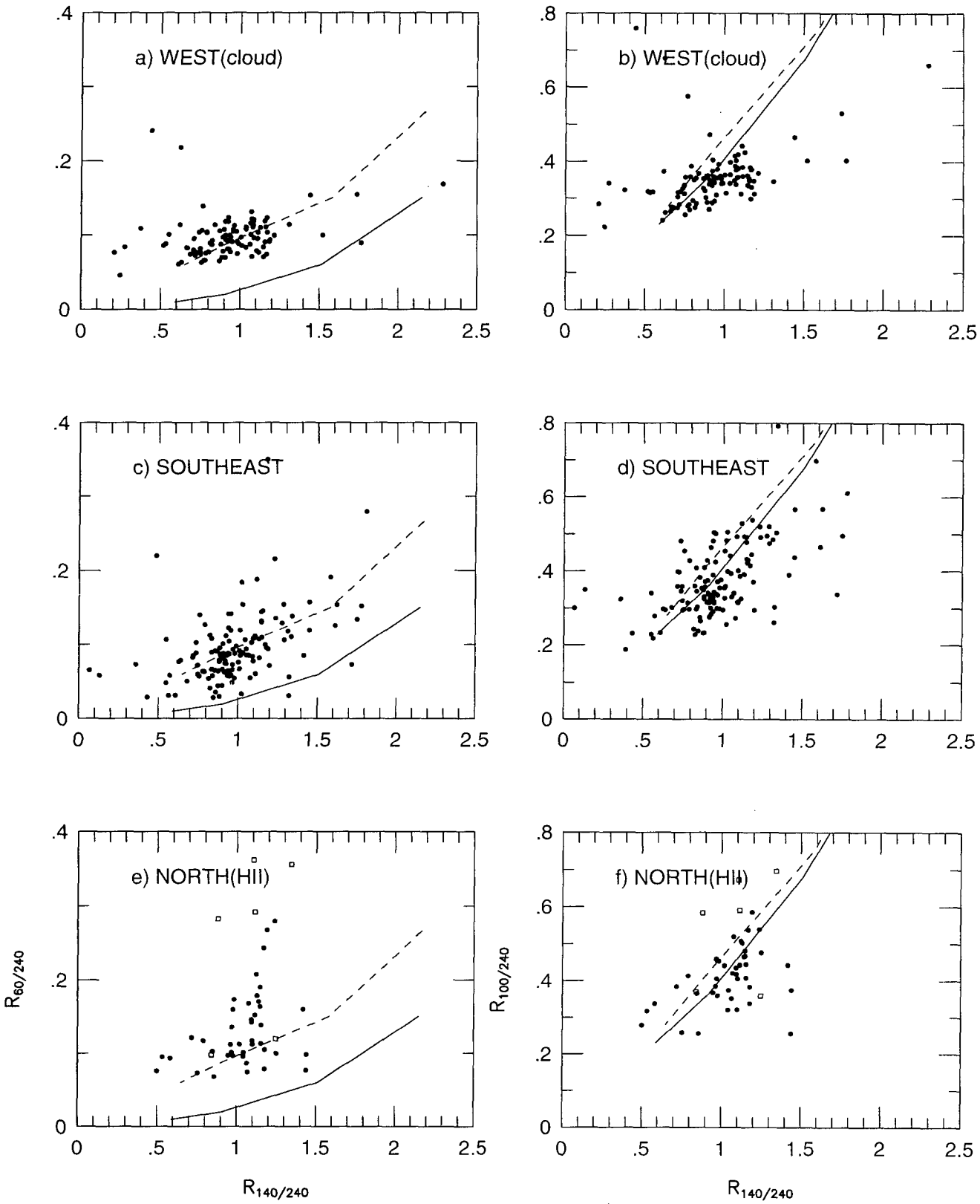

Fig. 5. Plots of FIR colors for each region. Color relations derived from the model are plotted as dashed (VSGs + BGs) and solid (BGs only) lines. Symbol in e) and f) is the same as that in Figure 4.

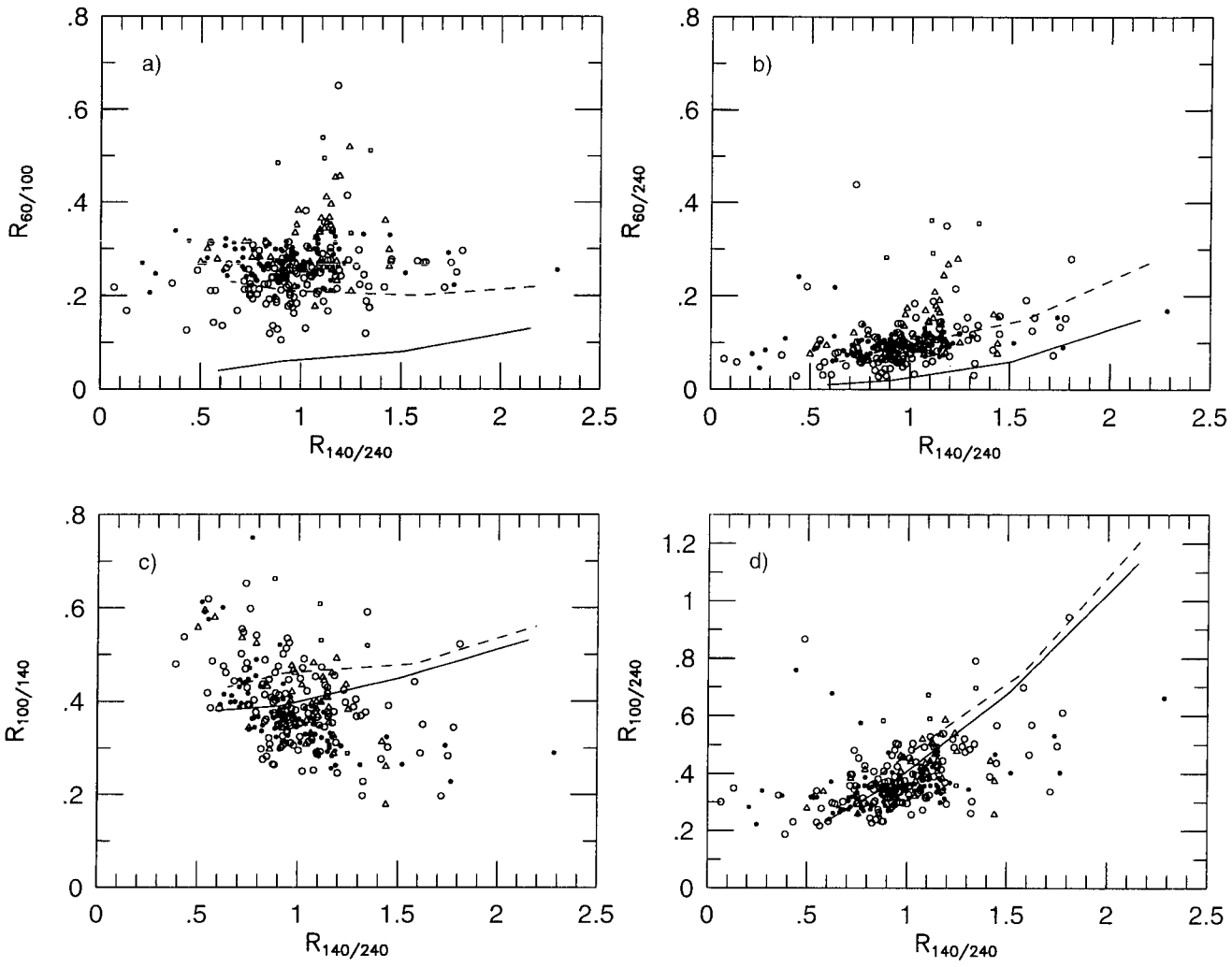

Fig. 6. Plots of FIR colors for all regions. The symbols are open squares for north1, filled triangles for north2, open circles for southeast, and filled circles for west region. Models are the same as those of Figure 5.

IV. EQUILIBRIUM TEMPERATURE OF BIG GRAINS

As we have seen in Figure 5, the contribution of VSGs is negligible at FIR, i.e., longer than 100 μm. It means that FIR emission arises from BGs in equilibrium with ambient ISRF. The fact that the color temperatures, $T_{100/140}$ and $T_{140/240}$ are nearly same (see Table 1) also seems to support it.

In order to examine that BGs are really in equilibrium with ISRF, all IR colors derived from COBE data are plotted in Figure 6. Figure 6 shows that observed colors agree well with theoretical ones. Unlike for other colors, however, the observed $R_{100/140}$ in Figure 6c decreases with respect to $R_{140/240}$ whereas theoretical one increases. Although it is uncertain whether or not the anti-correlation between two colors is a general characteristic of the interstellar medium, it cannot be explained by thermal radiation of BGs. The anti-correlation may appear if the 140 μm emission changes with temperature much more sensitively than the emission in other bands.

A possible explanation is the enhancement of dust grain which emits most emission near 140 μm. Such a grain size distribution would have a extinction curve which is different from the observed one. Since DBP, however, derived the power law size distribution from the observed extinction curve of solar neighborhood, the modification of usual power law distribution is not highly recommended. An alternative is the introduction of a new type dust grain, which has different composition, or different mantle structure, or different albedo, etc. At the present we cannot suggest what nature it should have. And it is even uncertain that this type of dust grain could exist. Only more

observations, particularly for high temperature region where there exists big difference between the observations and the models, could provide information for the existence and characteristics of new dust grain.

In the case of anti-correlation of $R_{100/140}$, $T_{100/140}$ underestimates the equilibrium temperature and $T_{140/240}$ overestimates at high ISRF, while $T_{100/140}$ overestimates and $T_{140/240}$ underestimates at low ISRF. Therefore it might be safe to use $T_{100/240}$ as a dust thermometer although it gives only the upper limit because of the contribution of small particles at 100 μm.

V. SUMMARY AND CONCLUSIONS

Dust properties of molecular clouds were examined from their IR colors. In spite of different ISRF, we could not find any systematic difference of colors between them. This suggests that variations of IR colors are mainly due to the variations of dust abundance rather than the change of ISRF. Mean IRAS colors were estimated to be $R_{12/100}$= 0.074, $R_{25/100}$= 0.052, $R_{60/100}$= 0.219. The value $R_{12/100}$= 0.074 is about two times larger than that of the solar neighborhood, while the other colors are nearly the same as the local values. This implies that the abundance of PAHs is enhanced in the molecular clouds of GS234−02.

Separation of $R_{25/100}$ color was found in southeast region but not in north. This difference is interpreted by the opacity difference. Although both regions contain HII regions, the southeast region is much diffuser than north. Thus UV photons penetrate deeper into the cloud in southeast region, and much VSGs near and/or in HII regions are heated to high temperature. But north cloud shields UV photon more effectively and most 25 μm emission comes from the dust grains inside the cooler cloud.

Dust optical depth and dust color temperature at 240 μm in the region where no internal heating source exists are $\tau_{240} = 9.0 \pm 5.7 \times 10^{-4}$ and $T_{140/240}$= 15.4±1.5 K, and they agree well with those determined for the outer Galaxy by Sodroski *et al.*(1994). The dust temperature determined from the ratio between 140 and 240 μm, however, may not represent the equilibrium temperature, since $R_{100/140}$ shows the anticorrelation with $R_{140/240}$. This anticorrelation cannot be explained by thermal emission of big grains. To explain it, a new type of grain is invoked but the properties are unknown. One characteristic of this new type of grain is that its emission peak may be at 140 μm and its emissivity is sensitive to temperature. The anticorrelation of $R_{100/140}$ implies that $T_{140/240}$ overestimates the equilibrium temperature at high ISRF but underestimates it at low ISRF. Therefore we propose to use the intensity ratio of 100 μm to 240 μm as a dust thermometer even though it gives only an upper limit.

ACKNOWLEDGEMENTS

We appreciate Dr. Koo, Bon-Chul for many helpful comments, and Mr. Kim, Jongsoo for a careful reading of the manuscript.

REFERENCES

Beichman, C., Wilson, R. W., Langer, W., & Goldsmith, P. 1988, ApJ,332,L81
Bernard, J. P., Boulanger, F., Desert, F. X., & Puget, J. L. 1992,A&A, 263,258
Boulanger, F., & Perault, M., 1988,ApJ,330,964
Boulanger, F., Falgarone, E., Puget, J. L., & Helou, G. 1990, ApJ,364,136
Chlewicki, G., & Laureijs, R. J. 1988,A&A,207,L11
Desert, F. X., Boulanger, F., & Puget, J. L. 1990,A&A,237,215(DBP)
Drain, B. T., & Anderson, N. 1985,ApJ,292,494
Heiles, C., Reach, W. T. , & Koo, B-C 1988,ApJ,332,313
Jung, J. H. 1996, Ph.D. thesis, Kyungpook National University (Korea)
Jung, J. H., Koo, B-C, & Kang, Y-H 1996,AJ,112,1625
Laureijs, R. J., Chlewicki, G., Clark, F. O., & Wesselius, P. R. 1989, A&A,220,226

Laureijs, R. J., Clark, F. O., & Prusti, T. 1991,ApJ,372,185
May, J., Murphy, D. C., & Thaddeus, P. 1988,A&AS,73,51
Puget, J. L. 1989, in IAU Symposium 135, Interstellar Dust, ed. L. J. Allamandola and A. G. G. M. Tielens (Kluwer Academic Publisher), p. 119
Puget, J. L., Leger, A., & Boulanger, F. 1985,A&A,142,L19
Schwartz, P. R. 1987,ApJ,320,258
Sivans, J. P. 1974,A&AS,16,163
Sodroski, T. J., Dwek, E., Hauser, M. G., & Kerr, F. J. 1989, ApJ,336,762
Sodroski, T. J., *et al.*. 1994,ApJ,428,638
Terebey, S., & Fich, M. 1986,ApJ,309,L73
Weiland, J. L., Blitz, L., Dwek, E., Hauser, M. G., Magnani, L., & Rickard, L. J. 1986,ApJ,306,L101
Werner, M. W., and Gautier III, T. N. 1994, in ASP Conference Series, Vol. 58, p.270
Wheelock, S., *et al.*. 1994, IRAS Sky Survey Atlas